The Characteristics of Lamina Cribrosa Defects in Myopic Eyes With and Without Open-Angle Glaucoma

Jong Chul Han, Seok Ho Cho, Dae Yong Sohn, and Changwon Kee

Department of Ophthalmology, Samsung Medical Center, Sungkyunkwan University School of Medicine, Seoul, Korea

Correspondence: Changwon Kee, Department of Ophthalmology, Samsung Medical Center, Sungkyunkwan University School of Medicine, 81 Irwon-ro, Gangnam-gu, Seoul 135-710, Korea;
ckee@skku.edu.

Submitted: July 17, 2015
Accepted: December 18, 2015

Citation: Han JC, Cho SH, Sohn DY, Kee C. The characteristics of lamina cribrosa defects in myopic eyes with and without open-angle glaucoma. *Invest Ophthalmol Vis Sci*. 2016;57:486–494. DOI:10.1167/iovs.15-17722

Purpose. We investigated the lamina cribrosa (LC) structural characteristics of myopic eyes with and without open-angle glaucoma (OAG) using enhanced depth imaging spectral-domain optical coherence tomography (EDI SD-OCT).

Methods. Defects in the LC in myopic eyes with and without OAG and normal eyes without myopia were evaluated using EDI SD-OCT. Among the two types of LC defects, disinsertion type and hole type, the associations among disinsertion type LC defects, myopia-related parameters of axial length (AL), maximal γ-zone peripapillary atrophy (PPA) length, disc tilt angle, and the presence of glaucoma were evaluated. In addition, disinsertion type LC defects were divided into two subtypes, complete detachment type and triangular wedge type, and the numbers of the subtypes in myopic eyes with and without OAG were investigated.

Results. Defects in the LC were found more in myopic eyes with than without OAG (65.7% vs. 27.8%, $P < 0.001$). Of LC defects, disinsertion-type LC defects were found at the location of the γ-zone PPA ($R = 0.71$, $P < 0.001$), while the location of hole-type LC defects did not correlate with the location of the γ-zone PPA ($R = 0.07$, $P = 0.73$). Of disinsertion-type LC defects, complete detachment-type defects predominated in myopic eyes with OAG, while triangular wedge-type defects were the most common in myopic eyes without OAG ($P < 0.001$; $P < 0.001$, respectively). In multivariate logistic regression analysis, disinsertion-type LC defects in myopic eyes were associated with AL, maximal PPA length, and disc tilt angle, as well as the presence of glaucoma.

Conclusions. Given the strong correlation of disinsertion type LC defects with glaucoma and parameters related to myopia, such defects should be considered as biomarkers of glaucoma in myopic eyes.

Keywords: lamina cribrosa, myopia, open-angle glaucoma, lamina cribrosa defect, lamina disinsertion

Myopia is associated with glaucoma prevalence; however, the causes of this association have not yet been discovered.[1–7] Morphologically, thin β-zone peripapillary atrophy (PPA) and optic disc tilt have been found to be characteristic of the optic nerve head (ONH) of myopic eyes.[8–11] Furthermore, β-zone PPA and optic disc tilt have been suggested as factors associated with the development of retinal nerve fiber layer (RNFL) defects in glaucomatous eyes.[12,13] The location of β-zone PPA and disc tilt direction were reported to be consistent with the site of RNFL defects in glaucoma.[14–16]

The lamina cribrosa (LC), an array of collagen beams with intervening pores, is the primary site of glaucomatous damage.[17,18] Histologic studies have shown that glaucoma or increased IOP induce LC thinning, posterior displacement, deformation, and lamina defects.[19–22] According to in vivo imaging studies, similar results have been found in glaucomatous eyes.[23–25] Recently, several studies have demonstrated the relationship between LC defects and glaucoma.[22,26] In addition, Takayama et al.[27] suggested that myopia was associated with the prevalence of LC defects. However, evidences have not yet been suggested enough to support the possible associations among LC defect, myopia, and glaucoma.

Recently developed spectral-domain optical coherence tomography (SD-OCT) enables in vivo cross-sectional visualization of the optic disc structures, including the Bruch's membrane (BM), border tissue of Elschnig, and PPA. Previously, Jonas et al.[28] differentiated γ-zone PPA from β-zone PPA based on the presence of BM in histologic study. By virtue of SD-OCT, the measurement of γ-zone PPA also is clinically possible.[28] In the previous studies, β-zone PPA without BM (γ-zone PPA) was reported to be correlated with myopia.[8,28]

Therefore, we designed this study to understand the relations among LC defect, open-angle glaucoma (OAG), and myopia-related parameters, such as disc tilt and γ-zone PPA, using SD-OCT. We compared numbers, sizes, and morphologic characteristics of LC defects among normal eyes without myopia, and myopic eyes with and without OAG. In addition, we investigated whether an LC defect would be associated with myopia-related parameters, such as optic disc tilt or γ-zone PPA.

Methods

This was a cross-sectional observation study. Candidates of this study were patients with myopic eyes with and without OAG who visited Samsung Medical Center (Seoul, South Korea) between January 2014 and December 2014. Normal eyes without myopia were included as normal controls who had undergone glaucoma screening test for check-up in Samsung Medical Center. This study followed all guidelines for experimental investigation in human subjects, was approved by the

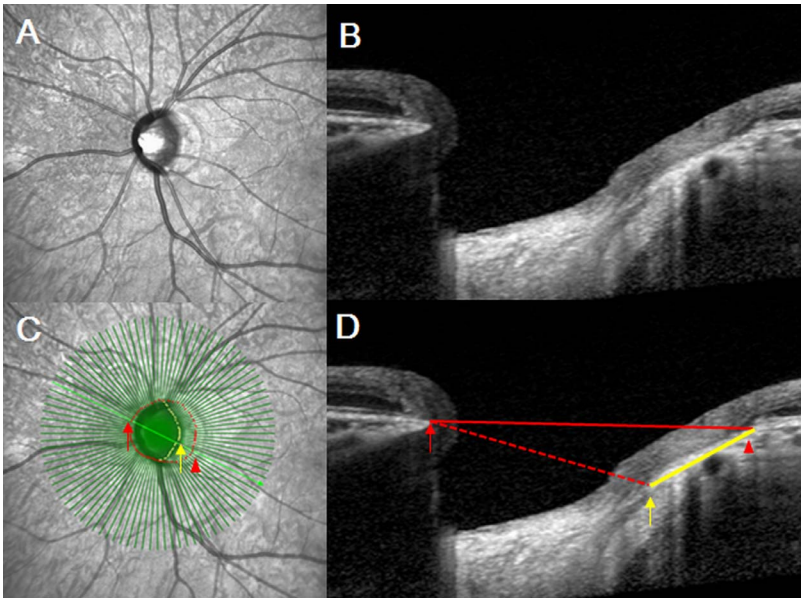

FIGURE 1. Measurement of the optic disc tilt parameters using EDI OCT. (**A**) Infrared photography included in EDI OCT device shows en face images of ONH. (**B**) Enhanced depth imaging OCT offers a sectional image of ONH including LC. (**C**) Enhanced depth imaging OCT scan was obtained using 48 radial line B-scans (each at an angle of 3.75°). In each sectional image, the *dots* that are located at BMO were used as the reference BMO margin (*dotted red circle*) and the *dots* that are located at the end of externally oblique border tissue were defined as the temporal optic canal margin (*dotted yellow circle*). (**D**) Gamma zone PPA length (*solid yellow line*) was defined as the region between the temporal BMO (*red arrowhead*) and termination of the externally oblique border tissue (*yellow arrow*). The *line* that connects both BMOs (*red arrow* and *red arrowhead*) was used as the reference BMO plane (*solid red line*) and the *line* that connects nasal BMO (*red arrow*) and the end of externally oblique border tissue (*yellow arrow*) was defined as the optic canal plane (*dotted red line*). Disc tilt angle was defined as the angle between the BMO plane (*solid red line*) and the optic canal plane (*dotted red line*) at the maximum tilt location.

Samsung Medical Center Institutional Review Board, and adhered to the tenets of the Declaration of Helsinki.

Participants underwent a comprehensive ophthalmic assessment, including slit-lamp biomicroscopy, Goldmann applanation tonometry (GAT), manifested refraction, dilated stereoscopic examination of the ONH and color optic disc photography (Topcon, Paramus, NJ, USA), automated perimetry using the central 30-2 Humphrey Field Analyzer (HFA model 640; Humphrey Instruments, Inc., San Leandro, CA, USA), axial length (AL) measurement (IOL master; Carl Zeiss Meditec, Jena, Germany), and ultrasound pachymetry (Tomey SP-3000; Tomey Ltd., Nagoya, Japan). The extent of visual field (VF) defects was measured using the mean deviation (MD), pattern standard deviation (PSD), and visual field index (VFI). Reliable VF analysis defined as a false-negative rate $<15\%$, a false-positive rate $<15\%$, and fixation loss $<20\%$ was used.

The following criteria were required for the diagnosis of OAG. First, glaucomatous optic disc changes, such as increased cupping (vertical cup-to-disc ratio > 0.7), diffuse or focal neural rim thinning, disc hemorrhage, or RNFL defects, were required at the time of diagnosis. Second, glaucomatous VF defects positive for at least two of the following criteria were required to have been present during more than one reliable test: a cluster of three points with a probability less than 5% on the pattern deviation map in at least one hemifield, including at least one point with a probability less than 1% or a cluster of two points with a probability less than 1%; a glaucoma hemifield test result outside the normal limits; or a pattern standard deviation of 95% outside the normal limits. Third, an open angle on gonioscopic examination must have been confirmed with no identified causes of secondary glaucoma present. Normal healthy eyes required a best-corrected visual acuity of $\geq$20/40, open angles on the gonioscopic exam, an IOP between 10 and 21 mm Hg, no glaucomatous optic disc, and VF changes.

To be classified with myopic eyes, the eyes also had to have a spherical equivalent (SE) less than -2.00 diopters and an AL greater than 24.0 mm. The participants were divided into three groups: myopia with and without OAG and normal eyes without myopia. Exclusion criteria included eyes with media opacities, such as a corneal opacity, cataract, or vitreous opacity, and systemic disease or ocular diseases that can affect VF tests. Only one eye in each patient was selected randomly in the present study.

Enhanced Depth Imaging OCT

The SD-OCT (Heidelberg Engineering, Heidelberg, Germany) was used to measure the LC. Heidelberg Spectralis OCT enhanced depth imaging (EDI) mode was used for all images. Imaging was performed within 6 months of VF testing. The device was pushed closer to the eye to move the zero reference plane more posteriorly, which enhanced the images of the deeper structures and created an inverted image, with the inner portions of the retina shown facing downward. The scans were performed using automatic real-time mode, which uses multiple line acquisition to reduce noise. The EDI scan was obtained using 48 radial line B-scans (each at an angle of 3.75°) centered on the optic disc, as reported previously.[29] Each EDI scan included the average of 20 OCT frames. We corrected the scaling of OCT machine into 1:1 μm before the measurement. Eyes were excluded if they had poor quality OCT images that did not offer information on LC morphology. A poor-quality image was defined as a scan with $<70\%$ of the anterior LC visible due to prelaminar tissue, RPE, or overlying vessels in $\geq$3 of the 48 radial line scans.

Measurement of Parameters Related to Myopic Tilted Disc and Gamma Zone PPA

We used the OCT anatomy to measure the myopic disc tilt. Infrared (IR) photography using a confocal scanning laser

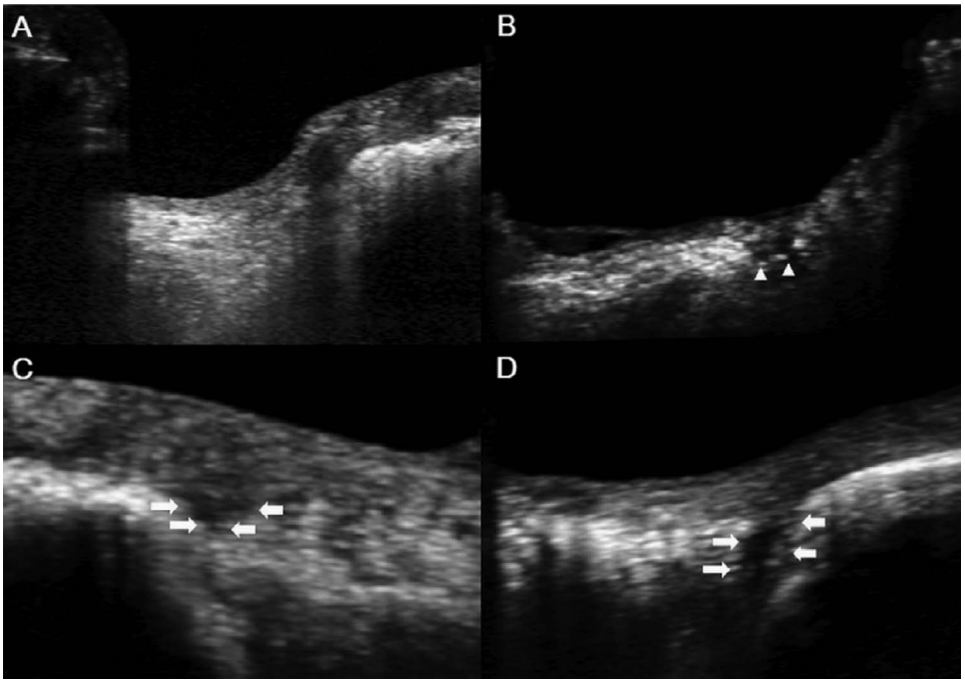

Figure 2. Types of LC defects. (**A**) The shadow that mimics an LC defect actually is a result of peripheral prelaminar tissue and overlying vessels. Shadowing due to obstacles is characteristically directed posteriorly (*dotted arrows*) under prelaminar tissue and overlying vessels. (**B**) A hole-type LC defect appearing as a localized discontinuity of LC tissue at the midperiphery of the LC (*arrowhead*). (**C**) A disinsertion-type LC defect (*white arrows*). A triangular wedge-type defect (**C**) located at the far periphery of the LC showing a detached LC at the anterior border and an attached LC at the posterior border. (**D**) A complete detachment-type defect located at the far periphery of the LC and showing a complete peripheral LC defect.

ophthalmoscope (CSLO) included in SD-OCT and radial section scan were used for the measurement of the myopic disc tilt (Figs. 1A, 1B). The BM opening (BMO) margin was regarded as the region between the terminations of Bruch's membrane at the optic nerve head. The BMO areas were measured by ImageJ software (version 1.52, http://imagej.nih.gov/ij/; provided in the public domain by the National Institutes of Health, Bethesda, MD, USA). The innermost margin of the externally oblique border tissue was demarcated on the en face image of the SD-OCT and regarded as the optic canal margin (Fig. 1C).[30] The γ-zone PPA length was defined as the region between the innermost margin of the externally oblique border tissue and

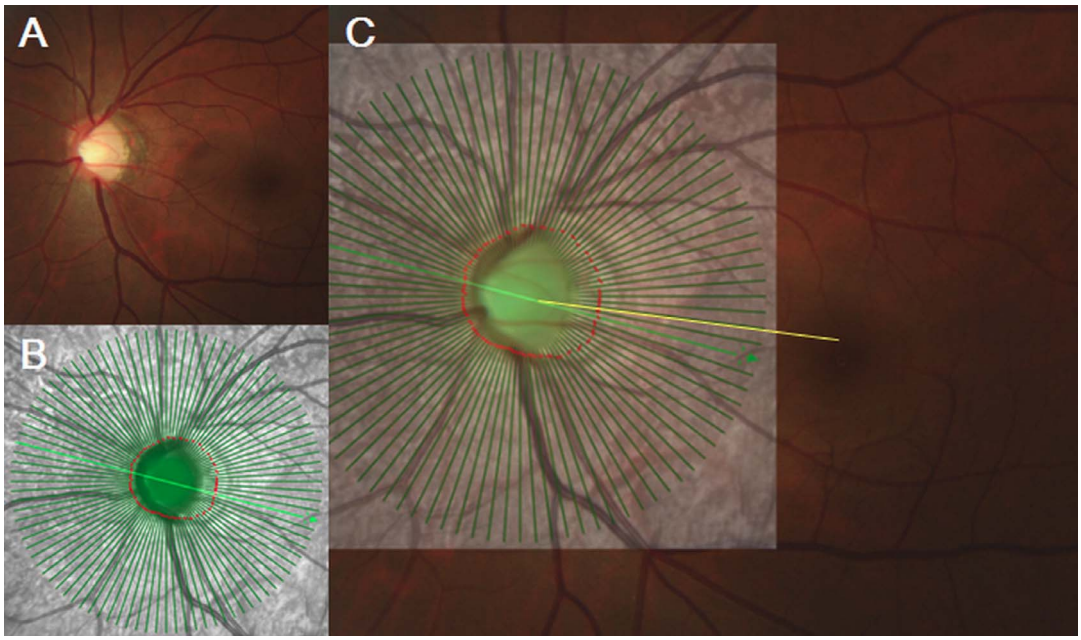

Figure 3. (**A**) A fundus photo that shows the locations of optic nerve head and fovea center. (**B**) The infrared en face EDI OCT image shows the locations of LC defects or γ-zone PPA. (**C**) Enhanced depth imaging OCT image for the same eye was superimposed on the fundus photo. The *line* connecting between BMO center to fovea (FoBMO axis) was defined as the reference line to set the location of LC defects or gamma zone PPA.

Investigative Ophthalmology & Visual Science

Table 1. Baseline Characteristics in Myopic Eyes With and Without Open-Angle Glaucoma

Parameters	Myopic Eyes With OAG, $N = 134$, A	Myopic Eyes Without OAG, $N = 90$, B	Normal Eyes Without Myopia, $N = 58$, C	*P* Value	Post Hoc Analysis		
					A vs. B	B vs. C	C vs. A
Age, y	50.9 ± 11.0 (31 to 79)	46.1 ± 11.0 (22 to 63)	51.3 ± 10.7 (33 to 71)	0.35			
Female sex, *n* (%)	86 (64.2)	51 (56.7)	32 (55.2)	0.38			
Ocular factors							
Initial IOP, mm Hg	17.3 ± 2.9 (11 to 23)	17.2 ± 2.5 (13 to 21)	16.5 ± 2.3 (10 to 21)	0.87			
SE, D	−5.2 ± 3.0 (−11.0 to −2.1)	−5.2 ± 2.7 (−10.0 to −2.1)	−1.2 ± 1.0 (−1.5 to 0)	0.03*	0.92	0.002*	0.002*
Axial length, mm	26.2 ± 1.5 (24.1 to 28.6)	26.0 ± 1.5 (24.3 to 28.4)	24.3 ± 1.4 (22.0 to 26.5)	0.03*	0.87	0.002*	0.001*
CCT, μm	531.6 ± 39.8 (426 to 609)	536.4 ± 36.4 (427 to 612)	530.5 ± 38.5 (455 to 602)	0.36			
Perimetric parameters							
MD, dB	−7.8 ± 6.0 (−17.1 to −1.0)	−1.7 ± 1.5 (−2.5 to 0.5)	−1.0 ± 0.6 (−1.7 to 0.5)	<0.001*	<0.001*	0.09*	<0.001*
PSD, dB	9.9 ± 4.6 (1.9 to 19.2)	2.1 ± 1.9 (0.9 to 4.7)	1.3 ± 1.1 (0.5 to 2.8)	<0.001*	<0.001*	0.04*	<0.001*
VFI, %	78.1 ± 18.4 (36 to 98)	99.5 ± 2.3 (98 to 100)	99.9 ± 1.0 (99 to 100)	<0.001*	<0.001*	0.89*	<0.001*
Optic disc parameters							
BMO area, mm^2	2.8 ± 0.7 (1.7 to 4.6)	2.5 ± 0.6 (1.7 to 4.3)	1.9 ± 0.2 (1.6 to 2.5)	<0.001*	0.83*	<0.001*	<0.001*
Maximal γ-zone PPA length, mm	1.0 ± 0.3 (0.5 to 2.4)	0.7 ± 0.2 (0.4 to 1.7)	0.1 ± 0.1 (0 to 0.3)	<0.001*	<0.001*	<0.001*	<0.001*
Disc tilt angle, deg	12.5 ± 5.1 (2.0 to 23.7)	10.1 ± 4.7 (1.5 to 20.3)	2.3 ± 1.7 (0.0 to 6.4)	<0.001*	0.02*	<0.001*	<0.001*

Values are shown in mean ± standard deviation (range) unless otherwise indicated. CCT, central corneal thickness; D, diopter; dB, decibel; EOBT, externally oblique border tissue.
* Statistically significant values.

the temporal BMO. Of the measured γ-zone PPA lengths, the largest measure was defined as the maximal γ-zone PPA length. The line connecting both BMO was regarded as the BMO plane and the line connecting nasal BMO and the innermost margin of the externally oblique border tissue was defined as the optic canal plane. The disc tilt angles were defined by the angle between the BMO plane and the optic canal plane at the maximum tilt direction (Fig. 1D). Assessment of the above parameters was performed independently by two glaucoma specialists (JCH and SHC) using ImageJ software.

Types, Numbers, and Sizes of LC Defects

A focal LC defect was defined as an anterior laminar surface irregularity violating the normal smooth curvilinear U- or W-shaped contour.[25] To avoid false-positives, true defects must have had a maximal diameter greater than 100 μm and a depth greater than 30 μm, and they must also have been present in two neighboring radial line scans.[25,29] Shadows were differentiated from LC defects in that they were characterized by a signal void behind the vessels and tissues (Fig. 2A). Lamina cribrosa defect margins were independent of the location of vessels and neural tissues. Focal LC defects were classified as holes or disinsertions. An LC hole was defined as a localized discontinuity of the LC tissue that usually was found at the mid-periphery of the LC (Fig. 2B). An LC disinsertion was defined as a posteriorly displaced laminar insertion with a downward slope at the far periphery of the LC toward the neural canal wall.[25] Furthermore, LC disinsertion types were classified as triangular wedge or complete detachment type using the revised definition from a previous report.[27] In the present study, a triangular wedge-type defect was a peripheral LC defect that showed a detached LC at the anterior laminar border and an attached LC at the posterior laminar border (Fig. 2C). A complete detachment type defect was defined as a complete peripheral LC defect from the anterior to the posterior margin (Fig. 2D). If an LC defect was identified after at least three sections with no defects, then it was considered a new LC defect. The mean number of LC disinsertions and holes and the total number of LC defects were investigated. The size of the LC defect was based on imaging showing the maximal length of the anterior LC defect surface.

The Locations of the γ-Zone PPA and LC Defects

The location of the γ-zone PPA and LC defects were measured with IR photography included in the SD-OCT. However, the fovea is not included in the SD-OCT optic disc scanning and BMO cannot be detectable in fundus photo; thus, we aligned the two images using Photoshop CS5; Adobe System, San Jose, CA, USA). The fovea-to-BMO (FoBMO) axis was defined as the line connecting the center of the BMO and fovea. The location of γ-zone PPA or LC defects was defined as the angle between the direction of maximal γ-zone PPA or LC defects and the FoBMO axis (Fig. 3).

Lamina cribrosa defect locations also were defined as a binary classifier. If the maximal LC defects were below the horizontal meridian of the optic disc, the location was regarded as inferior. Otherwise, the location of the LC defect was classified as superior. Assessments of LC defect location and size were performed independently by two glaucoma specialists (JCH and SHC) using ImageJ software. The final decisions regarding the presence, numbers, and types of LC defects were made through consensus agreement between the two readers.

Statistical Analysis

The intra- and interobserver (measured by JCH and SHC) reproducibility of parameters of BMO area, disc tilt angle,

Table 2. Intra- and Interobserver Reproducibility in Measurement of Parameters

	Intraobserver ICC (95% CI)	Interobserver ICC (95% CI)
BMO area	0.942 (0.875–0.964)	0.921 (0.799–0.957)
Disc tilt angle	0.902 (0.824–0.951)	0.897 (0.795–0.943)
Maximal PPA length, γ-zone PPA	0.951 (0.913–0.981)	0.941 (0.903–0.974)
PPA location, γ-zone PPA	0.930 (0.719–0.983)	0.903 (0.609–0.976)
The number of LC defects	0.837 (0.786–0.888)	0.811 (0.764–0.858)
LC disinsertion location	0.992 (0.981–0.999)	0.991 (0.975–0.999)
LC disinsertion size	0.973 (0.892–0.993)	0.971 (0.885–0.993)

maximal PPA length, and location (γ-zone PPA), the number of LC defects, LC disinsertion location, and size were assessed by calculating the intraclass correlation coefficients (ICCs). We used 20 randomly selected images in each parameter for the analysis. A 1-way ANOVA and Tukey's post hoc analysis were used to compare the variables among the groups. The number of eyes with LC defects between myopic eyes with and without OAG was compared using the χ^2 test. Because some myopic eyes had multiple LC defects, the mean numbers of LC defects per eye were compared between myopic eyes with and without OAG using the generalized estimating equation (GEE). Associations between the location of γ-zone PPA and LC defects were evaluated using Pearson's correlation approach. The correlation coefficient (R) also was calculated.

For both types of LC defects, the disinsertion-type LC defect size was compared between the two groups using the independent t-test, and the subtypes of LC disinsertion were compared using the χ^2 test. To investigate the factors associated with LC disinsertion in myopic eyes, univariate and multivariate logistic analyses were performed. The independent variables were CCT, initial IOP, AL, maximal PPA length, disc tilt angle, and presence of OAG. Parameters with a P value less than 0.1 in the univariate analysis were included in the multivariate logistic analysis model. All statistical analyses were performed using the Statistical Package for the Social Sciences (SPSS) software version 18.0 (SPSS, Inc., Chicago, IL, USA). A P value less than 0.05 was considered statistically significant.

Results

Of 153 patients with myopic eyes with OAG, 104 myopic eyes without OAG, and 68 normal eyes, 19 (12.4%), 14 (13.5%), and 10 (14.7%), respectively, were excluded because of poor imaging quality. No differences were found in age, sex, initial IOP, or CCT among the groups. The myopic eyes showed significantly different SE, AL, and BMO area compared to the normal eyes without myopia ($P = 0.03$, $P = 0.03$, $P < 0.001$). In myopic eyes, the myopia with OAG showed no significant differences in SE, AL, and BMO area compared to the myopic eyes without OAG, but maximal PPA length and disc tilt angle were larger in myopic eyes with than without OAG ($P < 0.001$, $P = 0.02$, respectively). The clinical characteristics of participants are compared in Table 1.

There was excellent agreement between graders as to whether an eye had an LC defect ($\kappa = 0.83$; 95% confidence interval [CI], 0.75–0.91; $P < 0.001$). The intra- and interobserver ICC showed good agreement for assessment of BMO area, disc tilt angle, maximal γ-zone PPA length, γ-zone PPA location, number of LC defects, LC disinsertion location, and size (Table 2). The normal eyes without myopia had no LC defects. In myopic eyes, LC defects were found even in the ones without OAG; however, the defects were more frequent in myopic eyes with OAG (27.8% vs. 65.7%; $P < 0.001$). Multiple LC defects also were identified more frequently in myopic eyes with than without OAG (25.4% vs. 6.7%; $P < 0.001$). The mean number of total LC defects and the disinsertion-type and hole-type LC defects per eye were higher in myopic eyes with than without OAG ($P < 0.001$, $P < 0.001$, $P = 0.002$, respectively; Table 3). The location of the LC disinsertion was correlated with the γ-zone PPA location ($R = 0.71$, $P < 0.001$; Fig. 3A). However, the location of the LC hole was not correlated with the γ-zone PPA location or maximal BMO distance location ($R = 0.07$, $P = 0.73$; Fig. 3B).

When only disinsertion-type LC defects were investigated, 88 myopic eyes with and 22 without OAG were included in the analysis. The LC disinsertion size was larger in myopic eyes with than without OAG (156.6 ± 41.6 vs. 130.5 ± 30.4 μm, respectively; $P = 0.01$). Among disinsertion-type LC defects, complete detachment was found more frequently in myopic

Table 3. Comparison of LC Defects Among the Groups

Parameters	Myopic Eyes With OAG, $N = 134$	Myopic Eyes Without OAG, $N = 90$	P Value
Eyes with LC defect, N	88 (65.7%)	25 (27.8%)	<0.001*
Eyes with multiple LC defects, N	34 (25.4%)	6 (6.7%)	<0.001*
Mean numbers of LC defects per eye, N	0.9 ± 0.1	0.3 ± 0.1	<0.001†
Superior	0.3 ± 0.0	0.1 ± 0.0	<0.001†
Inferior	0.7 ± 0.1	0.2 ± 0.1	<0.001†
Mean numbers of LC disinsertions per eye, N	0.7 ± 0.1	0.3 ± 0.1	<0.001†
Superior	0.1 ± 0.0	0.1 ± 0.0	0.02†
Inferior	0.6 ± 0.1	0.2 ± 0.1	<0.001†
Mean numbers of LC holes per eye, N	0.2 ± 0.0	0.0 ± 0.0	0.002†
Superior	0.1 ± 0.0	0.0 ± 0.0	0.003†
Inferior	0.1 ± 0.0	0.0 ± 0.0	0.001†

Values are shown in mean ± SD unless otherwise indicated.
* χ^2 test.
† Generalized estimating equation test.

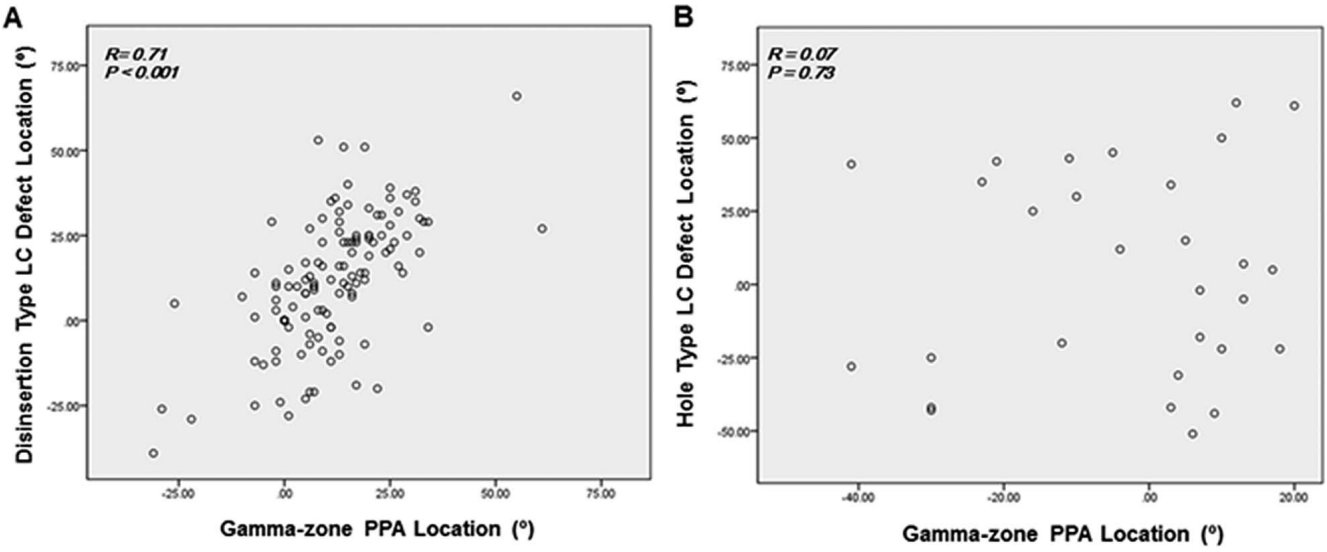

FIGURE 4. The correlation between the location of LC defect and γ-zone PPA and maximal BMO distance. Pearson's correlation coefficient (*R*) between the location of γ-zone PPA and a disinsertion-type LC defect (**A**) or a hole-type LC defect (**B**) was described in the graph.

eyes with than without OAG (73.9% vs. 27.3%, respectively; $P < 0.001$), and triangular wedge-type defects were seen more commonly in myopic eyes without than with OAG (72.7% vs. 26.1%, respectively; $P < 0.001$; Fig. 4, Table 4).

In the univariate logistic regression analysis, AL, maximal PPA length, disc tilt angle, and presence of OAG were related to the presence of disinsertion-type LC defects ($P < 0.001$, $P < 0.001$, $P = 0.03$, $P < 0.001$, respectively). Because maximal PPA size and disc tilt angle were strongly correlated (data not shown), multivariate analysis was performed separately using two models. In Model 1, AL, maximal PPA size, and presence of glaucoma were included in the analysis. Instead of maximal PPA size, disc tilt angle was included in Model 2 of the multivariate analysis. In multivariate logistic regression analysis, myopia-related parameters of AL, disc tilt angle, maximal PPA size, and presence of OAG showed significant association with presence of disinsertion-type LC defects (Table 5).

DISCUSSION

The present study revealed possible relationships among myopia, LC defects, and glaucoma. First, there were associations between myopia and disinsertion-type LC defects. Disinsertion-type LC defects were found even in myopic eyes without OAG. The myopia-related factors of AL, maximal γ-zone PPA length, and disc tilt angle also were associated with disinsertion-type LC defects. In addition, the location of γ-zone PPA was correlated with the location of LC disinsertion. Second, however, in myopia, OAG eyes had larger numbers and sizes of disinsertion type LC defects than the eyes without OAG. Furthermore, a larger proportion of complete detachment-type LC disinsertions were shown in myopic eyes with OAG than without OAG.

Myopia is a well-known risk factor for development of glaucoma. However, the reason why myopia induces glaucomatous defects has not yet been determined. Histologically, Jonas et al.[31] showed the presence of a thin LC and thin sclera in myopic eyes. In vivo imaging studies also have demonstrated a thin LC and thin scleral changes in myopic eyes.[32] Recently, myopic optic disc changes such as β-zone PPA, disc tilt, and torsion were suggested to be associated with glaucomatous defects.[16,33] The present study showed consistent results with the previous studies. Myopic changes around the ONH, such as maximal γ-zone PPA length or disc tilt angle, seem to be more important in producing glaucomatous RNFL defect than a longer AL itself in myopic eyes. No clear explanations have been suggested as to why PPA and disc tilt induce glaucomatous defects in myopic eyes. Previously, asymmetrical ultrastructural features between the superior and inferior LC and peripapillary sclera were suggested as the cause of increased vulnerability to IOP in the same eye.[16,34] However, few studies exploring the structural characteristics of the LC in myopic eyes have been performed to date.

Recently, LC defects have been shown to be associated with glaucoma. In these previous studies, LC defects were found in glaucomatous eyes but not in normal healthy eyes, and the location of these LC defects was consistent with glaucomatous changes in ONH and VF defects.[25,27,29,35] The present study results supported the hypotheses of previous studies in that LC

TABLE 4. Comparison of Disinsertion Type LC Between Myopic Eyes With and Without Open-Angle Glaucoma

Parameters	Myopic Eyes With OAG, $N = 88$	Myopic Eyes Without OAG, $N = 22$	*P* Value
LC disinsertion size, μm	156.6 ± 41.6	130.5 ± 30.4	0.01*
LC disinsertion type			
Complete detachment type, *n* (%)	65 (73.9)	6 (27.3)	<0.001†
Triangular wedge type, *n* (%)	23 (26.1)	16 (72.7)	

Values are shown in mean ± SD unless otherwise indicated.
* Independent *t*-test.
† χ^2 test.

Table 5. Logistic Regression Analysis: Variables Associated With the Disinsertion Type LC Defects

	Univariate Analysis			Multivariate Model 1			Multivariate Model 2		
Parameters	**OR**	**95% CI**	***P* Value**	**OR**	**95% CI**	***P* Value**	**OR**	**95% CI**	***P* Value**
CCT, μm	1.00	0.99–1.01	0.78						
Initial IOP, mm Hg	1.03	0.94–1.13	0.56						
AL, mm	1.42	1.17–1.72	<0.001	1.44	1.15–1.73	0.001	1.27	1.02–1.58	0.04
Maximal PPA length, mm	1.11	1.06–1.16	<0.001	1.41	1.27–1.55	<0.001			
Disc tilt angle, deg	1.52	1.17–1.87	0.03				1.23	1.12–1.34	0.007
Presence of OAG	5.91	3.25–10.76	<0.001	5.75	3.08–9.16	<0.001	5.71	3.05–10.74	<0.001

OR, odds ratio.

defects are associated with glaucoma. In the present study, LC defects were more frequent, multiple, and larger in myopic eyes with OAG than without OAG. The present study also showed the possible association between disinsertion type LC defects and myopia regardless of glaucoma based on the following reasons. First, LC defects were identified in more than one-quarter of myopic eyes without OAG. Second, disinsertion-type LC defects were associated with myopia-related parameters of AL, maximal γ-zone PPA length, and disc tilt angle. Third, the location of the LC disinsertion was correlated with the location of γ-zone PPA. The γ-zone PPA is the structure known as one of the myopia-related factors in the previous studies.[8,28] However, the reason why disinsertion type LC defects were found in glaucoma and myopic eyes is not certain. Given that myopic elongation may be related to optic disc tilt or γ-zone PPA, mechanical tensile strength may be involved in the formation of disinsertion-type LC defects.

The present study divided disinsertion type LC defects into two subtypes, such as complete detachment type and triangular wedge type, based on morphologic characteristics. In that disinsertion type LC defect located at the direction of γ-zone PPA, both subtypes seem to be related to myopic mechanical stress. In the present study, complete detachment types were dominant in myopic eyes with than without OAG. To explain the results, we propose the following possible hypotheses. First, the complete detachment type may be a result of greater tensile strength on peripheral LC than triangular wedge type. A mechanical overload on peripheral LC could make complete type LC disinsertion and induce instability on axon and blood vessels passing through it. Second, they might have a different mechanism associated not only with mechanical strength, but also with accompanying apoptotic changes or tissue remodeling on LC. Previous studies showed the possible mechanism, such as deformation and remodeling of the LC, that includes outward migration of the LC in experimental glaucoma model.[36–38] For such a mechanism, if an LC is exposed to stress or strain (mechanical strength) at the direction of PPA, the deformation and remodeling at the region can occur and lead to structural LC changes, such as initially wedge type LC disinsertions, and eventually complete detachment-type LC disinsertions.[38,39]

Investigators have used EDI OCT to better understand deep structures, such as LC or BM.[40] However, when investigating LC defects, there are several limitations. Retinal vessels or prelaminar tissues block the penetration of light and make it difficult to identify LC defects.[41] However, in eyes with myopic tilted discs, EDI OCT can offer good visualization of the junction between the LC and border tissues because tissues, such as Bruch's membrane and the retinal pigment layer at the tilt direction, usually are extended outside the disc margin.[30] In the present study, all eyes with myopic tilted discs showed externally oblique features in the tilt direction.

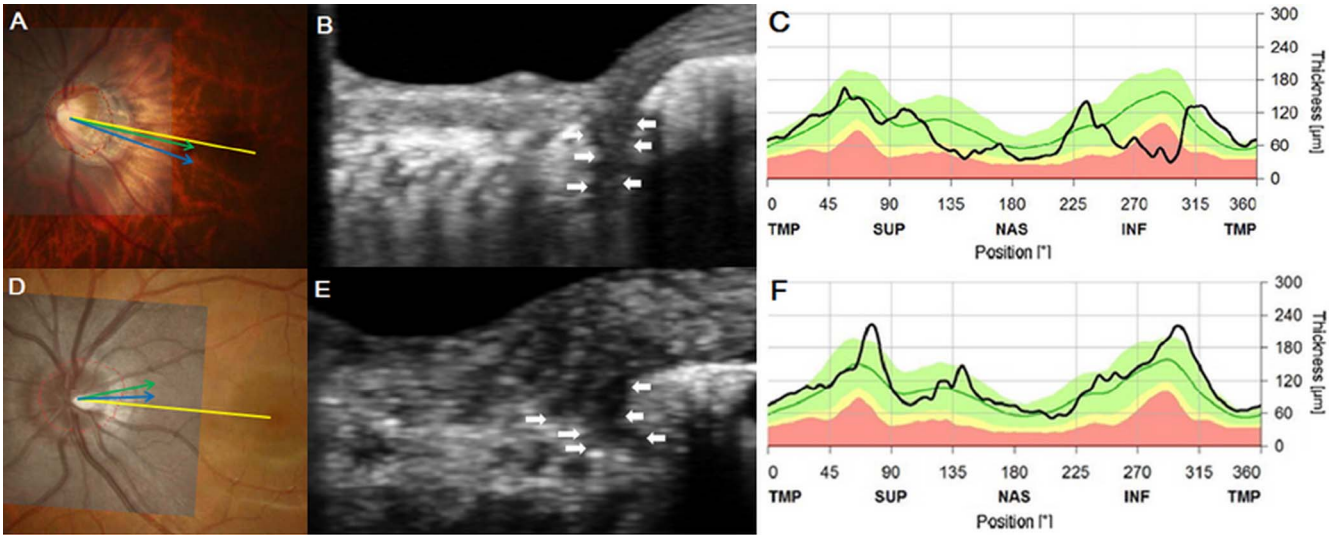

Figure 5. Representative cases showing a disinsertion-type LC defect at the location of γ-zone PPA in myopic eyes with OAG (**A–C**) and myopic eyes without OAG (**D–F**). (**A**) A myopic eye with OAG shows a γ-zone PPA location at 6° (*green arrow*) and a maximal LC disinsertion location at 14° (*blue arrow*). (**B**) A complete detachment-type LC disinsertion (*white arrow*) is shown at the γ-zone PPA location. (**C**) The location of a nerve fiber layer defect was consistent with γ-zone PPA location and LC disinsertion location. (**D**) A myopic eye without OAG eye shows a γ-zone PPA location at 28° (*green arrow*) and a maximal LC disinsertion location at 9° (*blue arrow*). (**E**) A triangular wedge-type LC disinsertion (*white arrow*) is shown at the γ-zone PPA location. (**F**) The RNFL thickness was within the normal range.

There are several limitations to the present study. First, it had a retrospective design. Second, the current findings have not yet been corroborated by histologic evaluation. To date, LC defects at the junction between the peripheral LC and scleral border have not been reported in histologic studies. Therefore, several defect types, such as optic pits, holes, and peripheral disinsertion types, have not been clearly defined and standardized previously. In the present study, several LC disinsertions less than 100 μm were found in glaucomatous and normal eyes with myopic tilted discs, though they were excluded from the analysis. In addition, the clinical meaning of hole-type LC defects in myopic tilted discs was not investigated. Future studies should examine whether there is clinical significance regarding LC defects based on size and type. Third, this study included only myopic eyes under −2.0 diopter and excluded several cases due to poor-quality images. A selection bias could have affected the results, though its impact on the results is uncertain. Furthermore, it might be difficult to observe defects in the center of the LC because the disc is tilted, resulting in less common identification of hole-type LC defects.

In conclusion, the present study showed that disinsertion type LC defects were associated with myopia-related factors of AL, maximal PPA length, and disc tilt angle, and with the presence of OAG using SD-OCT. In addition, the disinsertion type LC defects were found at the location of the γ-zone PPA. Therefore, the disinsertion-type LC defects are considered as one of the possible biomarkers of glaucoma in myopic eyes.

Acknowledgments

Disclosure: **J.C. Han**, None; **S.H. Cho**, None; **D.Y. Sohn**, None; **C. Kee**, None

References

1. Daubs JG, Crick RP. Effect of refractive error on the risk of ocular hypertension and open angle glaucoma. *Trans Ophthalmol Soc U K*. 1981;101:121–126.
2. Perkins ES, Phelps CD. Open angle glaucoma, ocular hypertension, low-tension glaucoma, and refraction. *Arch Ophthalmol*. 1982;100:1464–1467.
3. Mastropasqua L, Lobefalo L, Mancini A, Ciancaglini M, Palma S. Prevalence of myopia in open angle glaucoma. *Eur J Ophthalmol*. 1992;2:33–35.
4. Mitchell P, Hourihan F, Sandbach J, Wang JJ. The relationship between glaucoma and myopia: the Blue Mountains Eye Study. *Ophthalmology*. 1999;106:2010–2015.
5. Xu L, Wang Y, Wang S, Wang Y, Jonas JB. High myopia and glaucoma susceptibility the Beijing Eye Study. *Ophthalmology*. 2007;114:216–220.
6. Rose KA, Morgan IG, Smith W, Burlutsky G, Mitchell P, Saw SM. Myopia, lifestyle, and schooling in students of Chinese ethnicity in Singapore and Sydney. *Arch Ophthalmol*. 2008; 126:527–530.
7. Marcus MW, de Vries MM, Junoy Montolio FG, Jansonius NM. Myopia as a risk factor for open-angle glaucoma: a systematic review and meta-analysis. *Ophthalmology*. 2011;118:1989–1994.
8. Hayashi K, Tomidokoro A, Lee KY, et al. Spectral-domain optical coherence tomography of beta-zone peripapillary atrophy: influence of myopia and glaucoma. *Invest Ophthalmol Vis Sci*. 2012;53:1499–1505.
9. Ramrattan RS, Wolfs RC, Jonas JB, Hofman A, de Jong PT. Determinants of optic disc characteristics in a general population: The Rotterdam Study. *Ophthalmology*. 1999;106: 1588–1596.
10. Vongphanit J, Mitchell P, Wang JJ. Prevalence and progression of myopic retinopathy in an older population. *Ophthalmology*. 2002;109:704–711.
11. How AC, Tan GS, Chan YH, et al. Population prevalence of tilted and torted optic discs among an adult Chinese population in Singapore: the Tanjong Pagar Study. *Arch Ophthalmol*. 2009;127:894–899.
12. Jonas JB, Nguyen XN, Gusek GC, Naumann GO. Parapapillary chorioretinal atrophy in normal and glaucoma eyes. I. Morphometric data. *Invest Ophthalmol Vis Sci*. 1989;30: 908–918.
13. Jonas JB, Naumann GO. Parapapillary chorioretinal atrophy in normal and glaucoma eyes. II. Correlations. *Invest Ophthalmol Vis Sci*. 1989;30:919–926.
14. Cho BJ, Park KH. Topographic correlation between beta-zone parapapillary atrophy and retinal nerve fiber layer defect. *Ophthalmology*. 2013;120:528–534.
15. Lee KS, Lee JR, Kook MS. Optic disc torsion presenting as unilateral glaucomatous-appearing visual field defect in young myopic Korean eyes. *Ophthalmology*. 2014;121:1013–1019.
16. Choi JA, Park HY, Shin HY, Park CK. Optic disc tilt direction determines the location of initial glaucomatous damage. *Invest Ophthalmol Vis Sci*. 2014;55:4991–4998.
17. Minckler DS, Bunt AH, Johanson GW. Orthograde and retrograde axoplasmic transport during acute ocular hypertension in the monkey. *Invest Ophthalmol Vis Sci*. 1977;16: 426–441.
18. Quigley HA, Addicks EM, Green WR, Maumenee AE. Optic nerve damage in human glaucoma. II. The site of injury and susceptibility to damage. *Arch Ophthalmol*. 1981;99:635–649.
19. Jonas JB, Martus P, Horn FK, Junemann A, Korth M, Budde WM. Predictive factors of the optic nerve head for development or progression of glaucomatous visual field loss. *Invest Ophthalmol Vis Sci*. 2004;45:2613–2618.
20. Levy NS, Crapps EE. Displacement of optic nerve head in response to short-term intraocular pressure elevation in human eyes. *Arch Ophthalmol*. 1984;102:782–786.
21. Bellezza AJ, Rintalan CJ, Thompson HW, Downs JC, Hart RT, Burgoyne CF. Deformation of the lamina cribrosa and anterior scleral canal wall in early experimental glaucoma. *Invest Ophthalmol Vis Sci*. 2003;44:623–637.
22. Quigley HA, Hohman RM, Addicks EM, Massof RW, Green WR. Morphologic changes in the lamina cribrosa correlated with neural loss in open-angle glaucoma. *Am J Ophthalmol*. 1983; 95:673–691.
23. Park HY, Jeon SH, Park CK. Enhanced depth imaging detects lamina cribrosa thickness differences in normal tension glaucoma and primary open-angle glaucoma. *Ophthalmology*. 2012;119:10–20.
24. Strouthidis NG, Yang H, Downs JC, Burgoyne CF. Comparison of clinical and three-dimensional histomorphometric optic disc margin anatomy. *Invest Ophthalmol Vis Sci*. 2009;50: 2165–2174.
25. Kiumehr S, Park SC, Syril D, et al. In vivo evaluation of focal lamina cribrosa defects in glaucoma. *Arch Ophthalmol*. 2012; 130:552–559.
26. Feuerstein GZ, Wang X, Barone FC. The role of cytokines in the neuropathology of stroke and neurotrauma. *Neuroimmunomodulation*. 1998;5:143–159.
27. Takayama K, Hangai M, Kimura Y, et al. Three-dimensional imaging of lamina cribrosa defects in glaucoma using swept-source optical coherence tomography. *Invest Ophthalmol Vis Sci*. 2013;54:4798–4807.
28. Jonas JB, Jonas SB, Jonas RA, et al. Parapapillary atrophy: histological gamma zone and delta zone. *PLoS One*. 2012;7: e47237.

29. Tatham AJ, Miki A, Weinreb RN, Zangwill LM, Medeiros FA. Defects of the lamina cribrosa in eyes with localized retinal nerve fiber layer loss. *Ophthalmology*. 2014;121:110–118.
30. Reis AS, Sharpe GP, Yang H, Nicolela MT, Burgoyne CF, Chauhan BC. Optic disc margin anatomy in patients with glaucoma and normal controls with spectral domain optical coherence tomography. *Ophthalmology*. 2012;119:738–747.
31. Jonas JB, Berenshtein E, Holbach L. Lamina cribrosa thickness and spatial relationships between intraocular space and cerebrospinal fluid space in highly myopic eyes. *Invest Ophthalmol Vis Sci*. 2004;45:2660–2665.
32. Lopilly Park HY, Lee NY, Choi JA, Park CK. Measurement of scleral thickness using swept-source optical coherence tomography in patients with open-angle glaucoma and myopia. *Am J Ophthalmol*. 2014;157:876–884.
33. Rader J, Feuer WJ, Anderson DR. Peripapillary vasoconstriction in the glaucomas and the anterior ischemic optic neuropathies. *Am J Ophthalmol*. 1994;117:72–80.
34. Teng CC, De Moraes CG, Prata TS, et al. The region of largest beta-zone parapapillary atrophy area predicts the location of most rapid visual field progression. *Ophthalmology*. 2011;118:2409–2413.
35. You JY, Park SC, Su D, Teng CC, Liebmann JM, Ritch R. Focal lamina cribrosa defects associated with glaucomatous rim thinning and acquired pits. *JAMA Ophthalmol*. 2013;131:314–320.
36. Yang H, He L, Gardiner SK, et al. Age-related differences in longitudinal structural change by spectral-domain optical coherence tomography in early experimental glaucoma. *Invest Ophthalmol Vis Sci*. 2014;55:6409–6420.
37. Strouthidis NG, Yang H, Fortune B, Downs JC, Burgoyne CF. Detection of optic nerve head neural canal opening within histomorphometric and spectral domain optical coherence tomography data sets. *Invest Ophthalmol Vis Sci*. 2009;50:214–223.
38. Burgoyne C. The morphological difference between glaucoma and other optic neuropathies. *J Neuroophthalmol*. 2015;35(suppl 1):S8–S21.
39. Taylor CA, Senchyna M, Flanagan J, et al. Role of eIF5A in TNF-alpha-mediated apoptosis of lamina cribrosa cells. *Invest Ophthalmol Vis Sci*. 2004;45:3568–3576.
40. Park SC, De Moraes CG, Teng CC, Tello C, Liebmann JM, Ritch R. Enhanced depth imaging optical coherence tomography of deep optic nerve complex structures in glaucoma. *Ophthalmology*. 2012;119:3–9.
41. Inoue R, Hangai M, Kotera Y, et al. Three-dimensional high-speed optical coherence tomography imaging of lamina cribrosa in glaucoma. *Ophthalmology*. 2009;116:214–222.

Investigative Ophthalmology & Visual Science